JOURNAL OF PLANKTON RESEARCH | VOLUME 34 | NUMBER 9 | PAGES 790–801 | 2012

Enhanced nitrate fluxes and biological processes at a frontal zone in the southern California current system

QIAN P. LI[1,2]*, PETER J. S. FRANKS[1], MARK D. OHMAN[1] AND MICHAEL R. LANDRY[1]

[1]SCRIPPS INSTITUTION OF OCEANOGRAPHY, LA JOLLA, CA 92093 USA AND [2]SOUTH CHINA SEA INSTITUTE OF OCEANOLOGY, CAS, GUANGZHOU 510301, PR CHINA

*CORRESPONDING AUTHOR: qian@coast.ucsd.edu

Received November 3, 2011; accepted in principle January 16, 2012; accepted for publication January 21, 2012

Corresponding editor: John Dolan

Processes that occur at mesoscale and submesoscale features such as eddies and fronts are important for marine ecosystem dynamics and biogeochemical fluxes. However, their impacts on the fate of biogenic organic carbon in coastal oceans are not well quantified because physical and biological interactions at such features are very complex with short time- and small spatial scales variability. As part of the California Current Ecosystem Long-Term Ecological Research (CCE-LTER) Process studies in the southern California Current in October 2008, we sampled across a strong temperature and chlorophyll front ('A-Front') separating water masses with distinct hydrographic and biogeochemical characteristics and a modified biological assemblage at the frontal interface. Thorpe-scale analyses of the hydrographic data from a free-fall moving vessel profiler suggested an increased diapycnal diffusive nitrate flux at the front zone. Based on these field data, we use data-driven diagnostic biogeochemical models to quantify how the front-induced physical mixing influenced the production, grazing and transport of phytoplankton carbon in the southern California Current. Our results suggest that enhanced diffusive diapycnal fluxes of nutrients stimulated phytoplankton primary production at the front; this effect, together with reduced microzooplankton grazing, increased net growth of the phytoplankton community leading to locally enhanced biomass of large phytoplankton, such as diatoms, in the frontal zone.

KEYWORDS: nitrate fluxes; diatom; grazing; biogeochemical modeling; A-Front; frontal zone

INTRODUCTION

Studies of biogeochemical processes in marine ecosystem are complicated by small-scale physical phenomena such as eddies, fronts and filaments, which are ubiquitous in the world's oceans. Physical dynamics at frontal zones (~10 km scales) including frontogenesis, eddy-induced friction, mixed-layer instabilities, ageostrophic instability and Ekman pumping (Franks, 1992a; Levy *et al.*, 2001; Mahadevan and Tandon, 2006) may lead to small-scale vertical motions of tracers such as nutrients, whose concentrations change rapidly with depth just below the mixed layer or euphotic zone. These spatially discrete and temporally episodic nutrient fluxes could play an important role in fueling primary production in regions where phytoplankton growth is nutrient limited. However, biological responses to nutrient fluxes in the open ocean may also involve complex trophic interactions within the pelagic food web (Thingstad *et al.*, 2005).

There is increasing evidence that oceanic fronts are important zones of enhanced diatom concentrations

doi:10.1093/plankt/fbs006, available online at www.plankt.oxfordjournals.org. Advance Access publication February 20, 2012

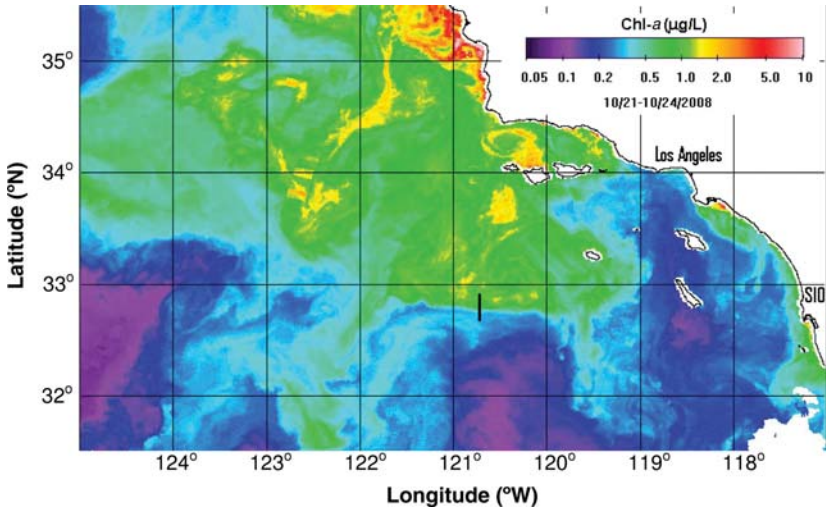

Fig. 1. Near-surface concentration of chlorophyll-*a* in the southern California Current System during the A-Front study (figure courtesy of M. Kahru, SIO). Black line illustrates the ~28 km south-north sections across the A-Front region.

and carbon sequestration in the ocean (Yoder *et al.*, 1994; Allen *et al.*, 2005; Kemp *et al.*, 2006). Diatom blooms are widely believed to be short-lived, because they are easily stimulated, limited and terminated by changes in inorganic nutrient inventories such as nitrate, silicate and iron (Hutchins and Bruland, 1998), as well as subject to grazing by diverse metazoans. When at least one of the ambient nutrients is exhausted, ungrazed diatom aggregations will sink out of the euphotic zone, exporting fixed organic carbon to the deep ocean. In the open ocean, processes such as upwelling at frontal zones and wind-eddy interactions can prolong the supply of new nutrients, sustaining diatom blooms (Allen *et al.*, 2005; McGillicuddy *et al.*, 2007) and enhancing their role in transferring carbon to the ocean interior as sinking particles or to higher trophic levels as food.

The Southern California Current System (SCCS) is a well-studied upwelling system that supports high biological productivity (Fig. 1). Since the beginning of the California Cooperative Oceanic Fisheries Investigations (CalCOFI) program in 1949, hydrographic and biological data collected in this area have improved our understanding of spatial and temporal patterns of physical and biological properties in the coastal and adjacent ocean waters of California. However, the advent of high resolution remote sensing and numerical models in recent decades (e.g. Brink *et al.*, 1991) has underscored the strong variability of the California Current Ecosystem (CCE) associated with eddies, fronts and filaments. The physical processes that generate and maintain these mesoscale/submesoscale features can directly induce upwelling/subduction and transfer coastal upwelled waters to offshore regions (Mooers and Robinson, 1984; Brink *et al.*, 1991; Levy *et al.*, 2001; Mahadevan and Tandon, 2006; Li *et al.*, 2008). Observations from autonomous gliders in the SCCS have confirmed that much of the patchiness of chlorophyll florescence is associated with vertical displacement of density fields induced by oceanic fronts (Davis *et al.*, 2008). Such small-scale features are not resolved by the current CalCOFI sampling grid. Thus, their roles in the dynamics of marine ecosystem and biogeochemistry in SCCS are still poorly understood.

In October 2008, we sampled a strong temperature and chlorophyll front in the southern sector of the California Current System that separated water masses with distinct hydrographic and biogeochemical characteristics, and displayed a markedly modified biological assemblage (including a diatom patch) at the frontal zone compared with each side of the front. Here, we combine data analyses and diagnostic biogeochemical models to address the linkages among vertical nutrient fluxes, organic carbon production, community structure and trophic dynamics at the front. In synthesizing these field and model results, our goal is to understand how the physical processes influence the planktonic community structure and ecosystem dynamics, and their potential roles in controlling biogeochemical fluxes in the southern California coastal pelagic ecosystem.

METHOD

Field work

On 24–25 October 2008, we sampled an intense submesoscale front (designated 'A-Front') in the SCCS

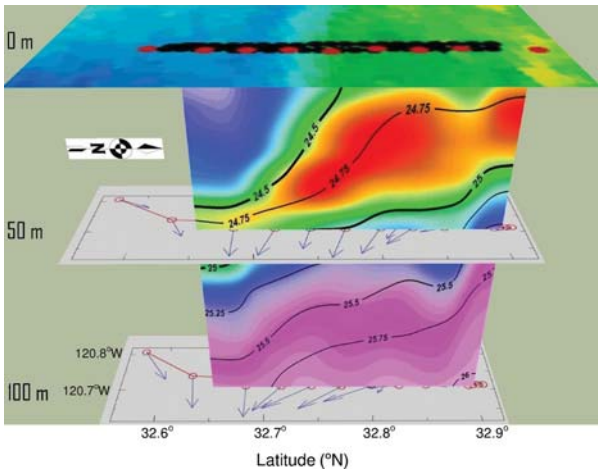

Fig. 2. Three-dimensional structure of the front transect. Three layers are shown with the map of sea-surface chlorophyll-*a* on the surface and the maps of ADCP currents (*arrows*) at 50 and 100 m depths. Section contour is the chlorophyll-*a* concentration in colors overlain by isopycnal surfaces as black lines. On the surface, red and black dots are the locations of the CTD stations and MVP (moving vessel profiler) stations, respectively.

having distinct temperature and chlorophyll signatures in the surface and subsurface (Figs 1 and 2). The A-Front region was first identified from daily MODIS/SeaWiFS imagery of sea surface temperature and chlorophyll-*a* (Landry *et al.*, 2012; Ohman *et al.*, 2012). The region was then surveyed with a moving vessel profiler system (MVP, ODIM Brooke Ocean; Ohman *et al.*, 2012) from the R/V *Melville* to determine the variability in water-column hydrographic characteristics across the front to a depth of 200 m (Fig. 2). The MVP is a free-fall vehicle that allows accurate and rapid underway collection of vertical profiles of conductivity, temperature, pressure (CTD) and laser optical particle counter profiles in the upper ocean. We used data from the CTD profiles for turbulence analyses, as described in the following section. During our first three front crossings, the MVP profiled vertically from the surface to 200-m depth with the ship steaming at 5–6 m s^{-1}. To increase the horizontal (cross-frontal) resolution of the MVP transect, we reduced the speed to ~3 m s^{-1} during our fourth and fifth MVP surveys. Immediately upon completion of the fifth crossing, we made vertical profiles at nine hydrographic stations on a transect from south to north across the front using a SeaBird 911 plus CTD rosette water sampler system. The SeaBird CTD was fitted with sensors to measure pressure, temperature, conductivity, fluorescence, dissolved oxygen and beam transmission. Bottle samples were collected for nutrient analyses using standard colorimetric methods and biomass and abundance of microplankton community based on flow cytometry and epifluorescence microcopy (for details of the methodologies see Taylor *et al.*, 2012). A 150 kHz ship-mounted acoustic Doppler current profiler (ADCP) was operating during our cruise, permitting near-continuous monitoring of upper ocean current structure.

Turbulence calculations and Thorpe analysis

In the absence of direct measurements of turbulent microstructure, a Thorpe-scale approach was used to estimate the dissipation rate of turbulent kinetic energy (Thorpe, 1977; Galbraith and Kelley, 1996; Thompson *et al.*, 2007; Gargett and Garner, 2008). This approach identifies and characterizes turbulent overturns in CTD profiles by calculating the vertical distance that a water parcel must be moved to keep it in stable equilibrium with the surrounding water—the Thorpe displacement (d_z): $d_z = d_f - d_i$, where d_f is the depth to which the point originally at d_i has been moved (Gargett and Garner, 2008). The Thorpe scale (L_T) can then be estimated as the root mean square of the Thorpe displacement: $L_T = (\Sigma d_z^2)^{0.5}$.

The dissipation rate of turbulent kinetic energy (ε) can be estimated from the Thorpe displacement and the stratification (Galbraith and Kelley, 1996; Thompson *et al.*, 2007):

$$\varepsilon = 0.64 \cdot L_T^2 \cdot N^3,$$

where the buoyancy frequency N is calculated as $N^2 = -g\rho_0^{-1}(\partial\rho/\partial z)$; g is the gravitational acceleration, and ρ_0 and $\partial\rho/\partial z$ are the average density and vertical density gradient across each overturn.

The diapycnal diffusivity (K_ρ) can be estimated by (Osborn, 1980)

$$K_\rho = 0.2 \cdot \varepsilon \cdot N^{-2}.$$

Finally, the vertical nutrient flux ($\mathcal{J}_n$) can be estimated as

$$\mathcal{J}_n = -K_\rho \cdot (\partial C/\partial z),$$

where C is the nutrient concentration, and $\partial C/\partial z$ is the vertical nutrient gradient. Nitrate concentrations for the MVP surveys were estimated from potential density based on a polynomial relationship derived by least-squares fitting of nitrate (determined from autoanalyzer measurements) and potential density (calculated from temperature and conductivity) from bottle samples acquired during the front transect ($r^2 = 0.99$, $n = 72$). Nitrate gradients were calculated from the potential density/nitrate relationship.

The accuracy of the Thorpe-scale approach for estimating the vertical overturns depends on errors associated with both data collection and interpretation (Galbraith and Kelley, 1996; Gargett and Garner, 2008). The effective resolution of MVP during cruises is 1–1.5 m with a fall rate of ~3.5 m s^{-1}, so we only included overturns >4.5 m (resolved by at least three good data points). Following previous studies, we use a series of criteria for selection of real overturns, including the Nyquist frequency/minimum thickness (rejecting overturns that are too small relative to the sampling interval) (Thompson *et al.*, 2007), the run-length and water mass tests (Galbraith and Kelley, 1996), as well as the overturn ratio test (Gargett and Garner, 2008). These criteria ensure that the difference between the maximum and minimum density within an overturn is greater than twice the density-measurement noise ($\delta\rho = 0.001$ kg m^{-3}). Also, the vertical length scale of a measured overturn must be larger than twice the vertical resolution (Nyquist theorem) and larger than a minimum thickness of $2(g/N^2)(\delta\rho/\rho_0)$ (Galbraith and Kelley, 1996; Thompson *et al.*, 2007). Following Thompson *et al.* (Thompson *et al.* 2007), we use a water-mass test criterion less strict than that of Galbraith and Kelley (Galbraith and Kelley, 1996) by a factor of 2. The overturn ratio, the ratio of the vertical distance occupied by positive or negative Thorpe displacements to the length of the overturn, was set to >0.2 (Gargett and Garner, 2008). The noise ground of the MVP/CTD sensor is ~0.5 m, which is mostly lower than the minimum thickness.

Ecosystem models

Diagnostic ecosystem models, including a primary production model (Li *et al.*, 2010) and a microzooplankton grazing model (Li *et al.*, 2011), were applied to the A-Front data to address the fate of biogenic carbon and its relationship with physical dynamics at the frontal zone.

The primary production model is a physiology-based model of plankton growth and chlorophyll-*a*/irradiance acclimation (Li *et al.*, 2010). It includes two phytoplankton functional groups: diatom and non-diatom phytoplankton (including dinoflagellates, cyanobacteria etc). The diatom growth rate (μ) in the model is expressed as a function of nutrients, temperature and light:

$$\mu = V_{\max} \cdot \phi(N, Si) \cdot \xi(T) \cdot \gamma(PAR),$$

where $V_{\max}$ is the maximum growth rate, and φ, ξ and γ are functions representing the growth response to variations in nutrient, temperature and light, respectively. For non-diatom phytoplankton, silicate limitation was not included in the nutrient quota. The phytoplankton chlorophyll to the carbon ratio (*Chl:C*) is modeled by solving a non-linear equation that describes the photoacclimation of phytoplankton under *in situ* temperature and nutrient concentrations (see Li *et al.*, 2010 for details, table 1 for parameter values).

As shown in Li *et al.* (Li *et al.* 2010), the phytoplankton growth rate (μ), chlorophyll to the carbon ratio (*Chl:C*), carbon biomass and community structure of the CCE can be satisfactorily simulated using field measurements of temperature, chlorophyll and nutrients. For the A-Front study, discrete measurements of temperature, chlorophyll and nutrients from the bottle samples were used as model input variables to calculate phytoplankton growth rates, community structure, carbon biomass and primary production across the front for both functional types.

Grazing by the microzooplankton on phytoplankton in the model (Li *et al.*, 2011) (G) is expressed as

$$G = g_{\max} \cdot f(P) \cdot \mathcal{Z},$$

where $g_{\max}$ is the maximal grazing rate, $f(P)$ is a non-linear functional response of grazing rate to ambient prey concentration and P and $\mathcal{Z}$ are the biomass of phytoplankton and microzooplankton, respectively. A Holling type II formulation is used for $f(P)$ in this study:

$$f(P) = \frac{P}{P + k},$$

where k is the half saturation constant for microzooplankton grazing. The parameter values can be found in table 1.

Phytoplankton-specific grazing mortality rates m, equal to G/P, can be estimated by

$$m = g_{\max} \cdot f(P) \cdot (\mathcal{Z}/P).$$

The grazing models were parameterized using 2007 CCE field data with a non-linear fitting technique and verified by data of 2006 CCE studies (Li *et al.*, 2011). These models give statistically robust estimates of the grazing dynamics of microzooplankton on phytoplankton in SCC, ranging from rich coastal upwelling to oligotrophic offshore waters. The parameterizations reflect the aggregate interactions of different assemblages of grazers and prey that arise under different environmental conditions, rather than the functional relationship for a specific assemblage.

RESULTS AND DISCUSSION

Hydrographic origin of A-Front

Similar to other geostrophic fronts observed in the SCCS (Davis *et al.*, 2008), A-Front showed a typical surface boundary between the warmer and low-chlorophyll southern/offshore waters and the colder, high-chlorophyll northern/coastal waters (Fig. 1). Backtracking from the A-Front region using daily-merged sea level height anomaly data (SLHA) from the AVISO satellite (http://las.aviso.oceanobs.com/las/servlets/dataset), the A-Front section was located at the northern edge of an anticyclonic eddy (with positive SLHA) where it abutted a nearby cyclonic eddy (with negative SLHA). The current direction was west to east along the front, with velocities of 0.2–0.3 m s^{-1} at depths of 50 and 100 m measured from the shipboard ADCP (Fig. 2). These eastward flows were higher in the front relative to the regions immediately to the south and north of the front. Consistent with satellite observations, high chlorophyll patches were generally observed to the north of the front where the $\sigma_\theta = 24.5$ isopycnal outcropped. A deep chlorophyll maximum was located between the $\sigma_\theta = 24.5$ and $\sigma_\theta = 25$ isopycnals south of the front and increased in concentration toward the frontal interface along the isopycnals (Fig. 2; see also Ohman *et al.*, 2012).

Influence of three water masses can be found across the A-Front transect, with waters exhibiting a subsurface, low-salinity feature south of the front, somewhat saltier and warmer water north of the front, and transitional waters in the frontal zone (Fig. 3). The salinity and T/S curves from the A-Front section both showed evidence of isopycnal mixing of southern and northern waters in the frontal zone (Figs 3 and 4a). This suggests that mesoscale/submesoscale processes such as those observed in the A-Front region are important for the formation of SCCS water by mixing of coastal upwelling and offshore waters.

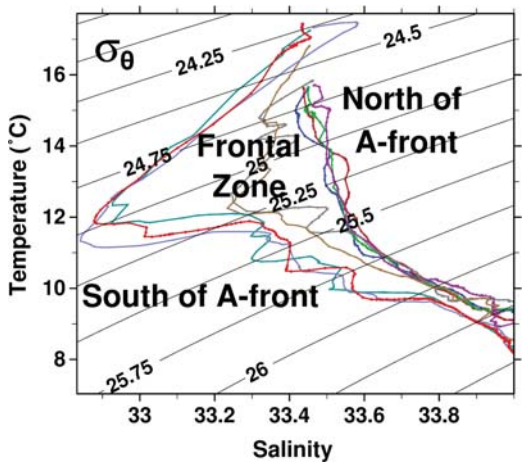

Fig. 3. Temperature-salinity diagram of the front. CTD data are illustrated from stations north of the A-Front region, south of the A-Front region, and the frontal zone.

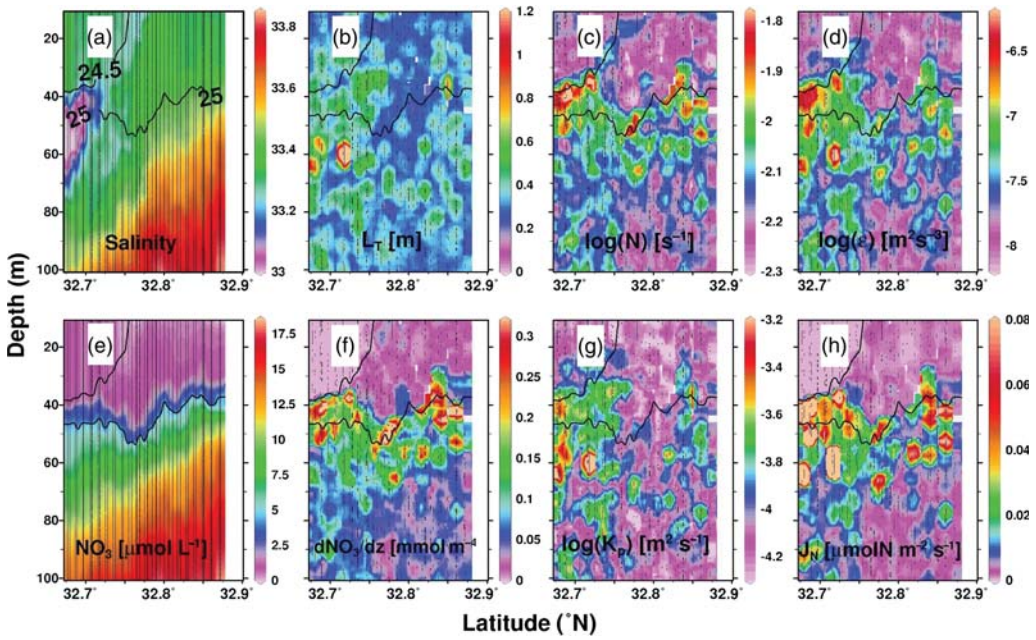

Fig. 4. Composite distributions of salinity (**a**), Thorpe scale (**b**), buoyancy frequency (**c**), energy dissipation rate (**d**), NO_3 concentration (**e**), vertical NO_3 gradient (**f**), diapycnal eddy diffusivity (**g**) and NO_3 fluxes (**h**) across the A-Front region from repeated MVP crossings of the front. The two thick lines in each panel are the $\sigma_\theta = 24.5$ and $\sigma_\theta = 25.0$ isopycnals, respectively. Vertical lines indicate the latitudes of MVP profiles, as indicated by black lines in Fig. 2.

Kahru *et al.* (Kahru *et al.* 2012) applied statistical techniques to analyze the frequency and time series of ocean fronts in the SCCS using satellite sea surface temperature and *Chl* data. Their results suggested that the large-scale distributions of frontal frequency (FF) showed a 500–700 km wide band of elevated values (4–7%) along the coast where increased mesoscale eddy activity was found. They also suggested that the major large-scale *Chl* fronts are quite consistent in space based on the monthly FF patterns, whose time series in coastal areas are positively correlated with the coastal upwelling index (Kahru *et al.*, 2012).

Diapycnal nitrate fluxes at the frontal zone

Diapycnal mixing can be an important source of nutrient fluxes to the euphotic zone because the vertical gradients of nutrients are strongest at the base of the euphotic zone. Diapycnal mixing in the ocean is generally presumed to be caused by small-scale turbulent processes associated with shear instabilities and internal wave breaking (Gargett and Garner, 2008). Approaches for quantifying diapycnal mixing often involve the measurement of small-scale turbulence using free-fall profilers for measuring density (Thorpe, 1977) and/or velocity microstructure (Gregg, 1989) or the penetration of a conservative tracer, such as SF_6, in the thermocline (Law *et al.*, 2003).

We applied Thorpe-scale analyses (Thorpe, 1977; Galbraith and Kelley, 1996; Gargett and Garner, 2008) to fine-scale MVP CTD profiles to determine the vertical turbulent length scale L_T (Fig. 4b), the turbulent kinetic energy dissipation rate ε (Fig. 4d) and the diapycnal eddy diffusivity K_ρ (Fig. 4g). Data within the surface mixed layer, approximately the upper 10 m, were discarded, as the Thorpe approach is not strictly valid there. In the upper 30–100 m relatively high K_ρ of 6.3×10^{-5} to 3.1×10^{-4} $m^2\ s^{-1}$ were observed. These high values were driven by large L_T (Fig. 4b) and high stratification (Fig 4c and g), and are consistent with other diapycnal diffusivity measurements in coastal regions (e.g. Hales *et al.*, 2005; Thompson *et al.*, 2007). Within the thermocline at 100–200 m (data no shown), we estimated diapycnal diffusivities from 1.6×10^{-5} to 5.0×10^{-5} $m^2\ s^{-1}$, which are slightly higher than the open ocean mean K_ρ of 1.0×10^{-5} $m^2\ s^{-1}$ (Munk and Wunsch, 1998; Law *et al.*, 2003). However, they are in good agreement with the K_ρ of 3.6×10^{-5} $m^2\ s^{-1}$ for an anticyclonic eddy estimated by a tracer dispersion experiment at the bottom of euphotic zone in the Sargasso Sea (Ledwell *et al.*, 2008). Although the spatial distribution of density overturns was very patchy across the A-Front region, as indicated from the patterns of Thorpe scales (Fig. 4b), the rates of diapycnal mixing and energy dissipation were much higher at the south side of the front than the north (Figs 4d and g). Interestingly, we also observed an increase of K_ρ and ε along the $\sigma_\theta = 24.75$ isopycnal from south of the front to the frontal zone (at ~35 m depth, Fig. 4g), where a patch of diatoms was found.

Diapycnal diffusive fluxes of nitrate (Fig. 4h) were predominately upward ranging from 0–0.48 μmol NO_3 $m^{-2}\ s^{-1}$ with a mean value of ~0.015 μmol NO_3 $m^{-2}\ s^{-1}$ at the base of euphotic zone. These fluxes are comparable with those found over the continental shelf off of the Oregon coast (Hales *et al.*, 2005) but higher than others observed in the open ocean (Law *et al.*, 2003; Ledwell *et al.*, 2008). Estimated diapycnal nitrate fluxes were generally elevated immediately below the band of high chlorophyll across the front section (Figs 2 and 4h) likely as a result of enhanced nutrient gradients driven by biological uptake (Fig. 4e and f) combined with enhanced vertical diffusivities there. Low nitrate fluxes within the high chlorophyll bands on the north side of the A-Front suggest that the observed phytoplankton patches (Taylor *et al.*, 2012) from past nutrient injection events might eventually decrease as they become more nitrogen limited and more dependent on recycled nitrogen. The high fluxes of nitrate in the deep chlorophyll maximum layer to the south of the front suggest that the growth of the phytoplankton community there may be limited less by nutrients than by other factors such as light availability or grazing pressure. The vertical nitrate flux at the base of euphotic zone in the frontal zone (~50 m depth; immediately below the diatom patch) was ~0.04 μmol NO3 $m^{-2}\ s^{-1}$, which could potentially support a new production of ~0.28 g C m^{-2} day^{-1} using a Redfield C/N ratio of 6.625. Total primary production measured in the same location (near CalCOFI Station 87.70) during previous CalCOFI studies ranges from 0.6 to 1.1 g C m^{-2} day^{-1} (seasonality included). Assuming an average f ratio of 0.36 in the Southern California Bight (Eppley, 1992), new production at the reference station could be 0.22–0.39 g C m^{-2} day^{-1}. Our estimated value of 0.28 g C m^{-2} day^{-1} from diapycnal nitrate flux thus falls within the above range.

Enhanced vertical mixing in the frontal zone may be explained by wind-forced dynamics at the front. The physical setting of A-Front (Fig. 2) is similar to the idealized geostrophic front of Franks and Walstad (Franks and Walstad, 1997), with isopycnal depression to the south and uplift to the north of the front and a strong along-front jet from west to east. During our surveys, winds of <7.5 m s^{-1} were generally blowing from northwest to southeast in alignment with the frontal jet. Such winds will force an Ekman flow from the cold dense side

of the front toward the warm less-dense side. This can create static density instabilities, as cold water is driven over warm water, that bring nutrients from the deep pool on the cold side of the front into the euphotic zone at the front (Franks and Walstad, 1997). As these static instabilities mix vertically, an opposing ageostrophic cross-frontal circulation will tend to re-stratify the front through a process called 'symmetric instability' (Hoskins, 1974; Thomas and Taylor, 2010; D'Asaro *et al.*, 2011). Curiously, this allows intense vertical mixing even while a vertical density gradient exists at the front; the mixed layer is both turbulent and stratified, even in the face of diapycnal mixing (D'Asaro *et al.*, 2011). Thus, our estimates of mixing at the front based on the Thorpe scale analysis are probably conservative, suggesting that the nitrate flux into the euphotic zone at the front could have been higher than calculated.

Phytoplankton growth and grazing mortality across the A-Front region

Using ecosystem models previously parameterized for the CCE (Li *et al.*, 2010, 2011), we estimated the growth and grazing of the phytoplankton community across the A-Front region. Unfortunately, there were no concurrent experimental measurements of phytoplankton growth and grazing rates from the A-Front region to test our model. However, during the same cruise, two sites, Cycle 5 (north of A-Front) and Cycle 6 (south of A-Front), were studied using a Lagrangian approach, following water masses with a drifting array, similar to previous process studies in the same region (Landry *et al.*, 2009). Cycle 5 showed a large net growth ($\mu - m$, where μ is specific growth and m specific death rate) of the phytoplankton community while phytoplankton growth and microzooplankton grazing were mostly balanced at Cycle 6. Comparison of our model results with data of Cycles 5 and 6 indicate that our model adequately reproduced the magnitudes and distributions of phytoplankton growth and grazing dynamics in this region during the 2008 cruise (Fig. 5), giving us some confidence in our predictions of biological rates at the front itself.

Although very patchy, modeled growth rates of the phytoplankton community generally showed a subsurface maximum across the A-Front region (Fig. 6e). Diatoms were more abundant north of the front, where high chlorophyll and phytoplankton carbon biomasses were found (Figs. 6a, h, k and l). The phytoplankton community south of the front was dominated by small phytoplankton such as phototrophic cyanobacteria (Taylor *et al.*, 2012), particularly *Prochlorococcus* which is small but grows efficiently in the warm (>15°C), low-nutrient surface waters of the offshore environments

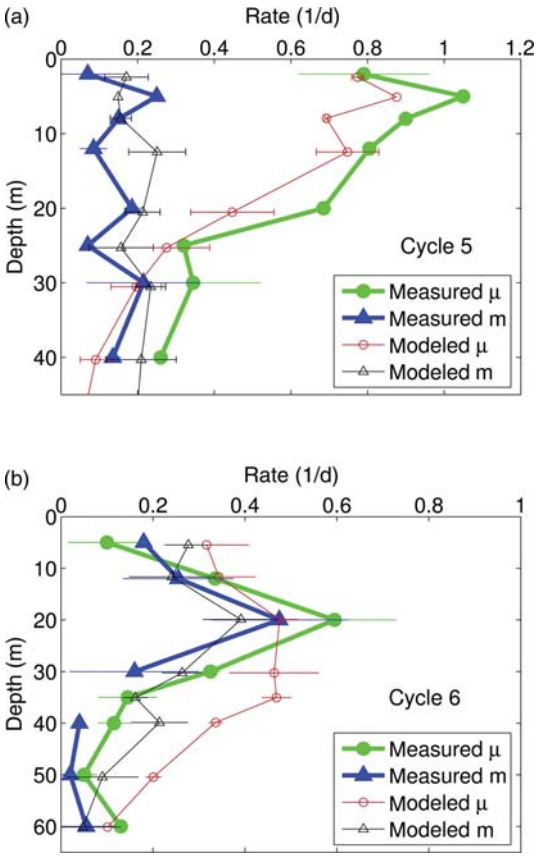

Fig. 5. Comparisons of modeled community growth and grazing rates with measured growth and grazing rates from seawater dilution experiments for Cycle 5 (north of the A-Front region) and Cycle 6 (south of the A-Front region). Filled symbols are measured data from dilution experiments; open symbols are output from the diagnostic model calibrated with independent data.

(Partensky *et al.*, 1999). While the biomasses were low south of the front, the model showed that the phytoplankton community there had high specific growth rates, consistent with our observation of high nitrate fluxes in the area (Fig. 4h). Our model suggests that community growth rates were not particularly high to the north of the front: the high phytoplankton concentrations there (Figs. 6e and k) led to reduced light in the upper euphotic zone. The lower chlorophyll and carbon biomasses south of the front allowed a deeper euphotic zone, resulting in higher community growth rates. However, the reduced light limitation of growth rate south of the front was balanced to some extent by the lower nutrient concentrations there. The role of iron in controlling diatom growth in the A-Front region is unknown, but the high variable fluorescence and dissolved iron concentrations at depth during the process studies suggested that it must be sufficient to allow photosynthetic production (Landry *et al.*, 2012; Ohman *et al.*, 2012).

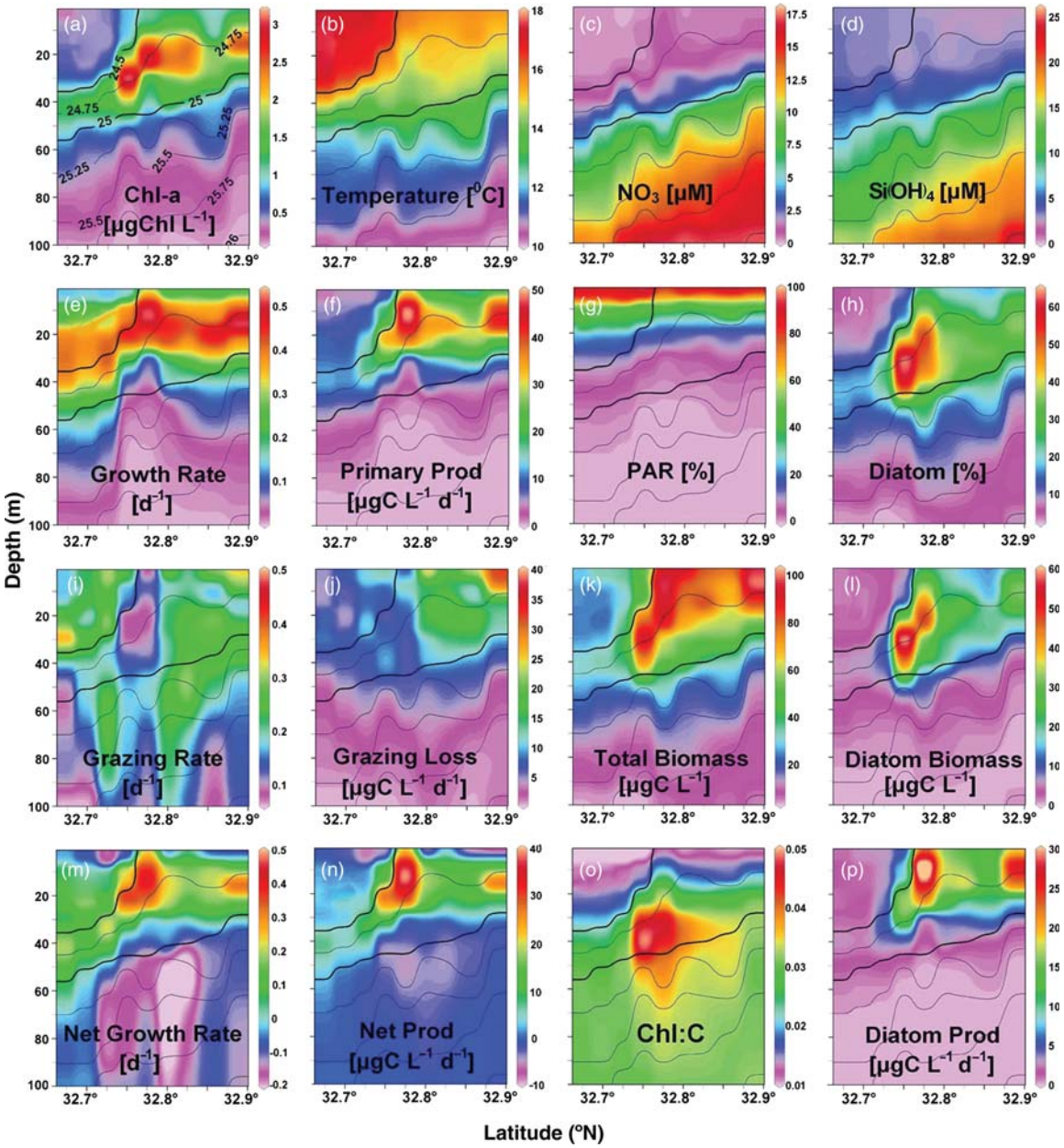

Fig. 6. Distributions of measured chlorophyll-*a* (**a**), temperature (**b**), NO_3 (**c**), $Si(OH)_4$ (**d**), and modeled community growth rate (**e**), primary production (**f**), PAR percentage (**g**), Diatom percentage (**h**), grazing mortality rate (**i**), grazing loss (**j**), total biomass (**k**), diatom biomass (**l**), net growth rate (**m**), net production (**n**), Chl:C ratio (**o**), and diatom production (**p**) across the front. Each panel is overlain with two isopycnal surfaces as thick black lines: $\sigma_\theta = 24.5$ and $\sigma_\theta = 25.0$, respectively.

Our model predicts a low grazing mortality of phytoplankton by microzooplankton in the frontal zone (see Fig. 6i), especially subsurface where the diatom patches were located. The specific grazing mortality rate of phytoplankton (m) is equal to $g_{max} \cdot f(P) \cdot (Z/P)$. Generally, $f(P)$ will be saturated when P is greater than a threshold value P_{80} (P at 80% saturation of $f(P)$ is equal to 0.5 μmol N L^{-1}). Therefore, m should be approximately proportional to Z/P when P is high ($P > P_{80}$). A lower Z/P ratio will result in a lower specific grazing rate in the model. It has been suggested that the ratio of Z/P (microzooplankton over phytoplankton) generally decreases with increase of P in both coastal and open oceans (Gasol *et al.*, 1997). Therefore, the specific mortality rate m will decrease with increasing autotrophic biomass P when P is high ($P > P_{80}$). This result helps us better understand the low modeled phytoplankton mortality in the frontal zone. Indeed, because biomass of

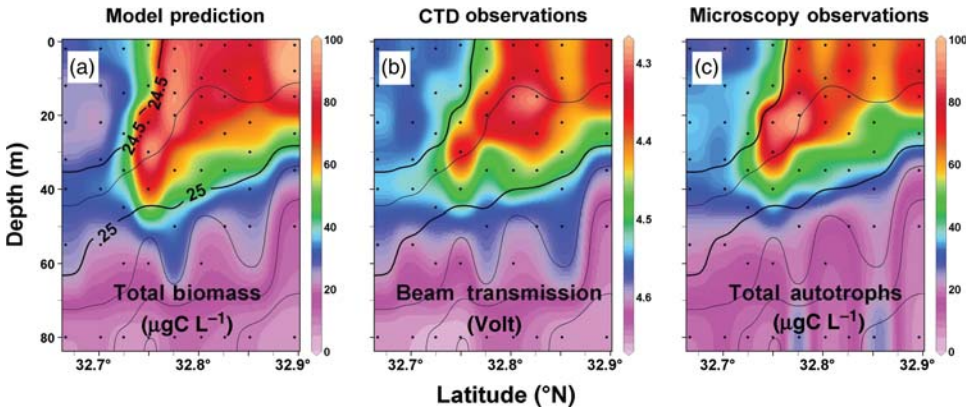

Fig. 7. Comparison of modeled total carbon biomass (**a**), beam transmission voltage from the CTD (**b**), and measured total autotrophic carbon biomass from FCM and EPI (**c**). Lines are as indicated in Fig. 6.

heterotrophic protists was not significantly enhanced at the frontal zone (Taylor *et al.*, 2012), the higher phytoplankton biomass there resulted in a lower $\mathcal{Z}/P$ ratio, which led to a lower specific grazing estimate in our model. The tendency of the $\mathcal{Z}/P$ ratio to decrease with increasing P in planktonic communities is probably the result of several factors, such as the change of autotroph turnover rates, predator suppression of protistan consumers, and reduced autotroph loss rate with eutrophication (Gasol *et al.*, 1997). Our present results suggest that the lower $\mathcal{Z}/P$ ratio at the frontal zone compared with each side of the front was due to increased phytoplankton community growth rate (Fig. 6m), which exceeded the capacity of microheterotrophs to fully exploit their production.

Our results also indicate that the pattern of net phytoplankton community growth rate ($\mu - m$) across the A-Front region is substantially different from those of the growth and the grazing rates alone (Fig. 6m and n). Phytoplankton growth was generally in excess of grazing mortality in the mid-euphotic zone but balanced in near-surface and deep layers. Although growth rate (μ) was not particularly high in the frontal zone, the net community growth rates ($\mu - m$) there were higher than on either side of the front, consistent with the observation of higher diatom biomass in the frontal zone (Taylor *et al.*, 2012) where diatoms were likely favored by increased nutrient fluxes that allowed them to sustain rapid growth rates. Our diagnostic models suggest that microzooplankton consumed only $47 \pm 12\%$ of the phytoplankton production (m/μ) at the front, which is significantly lower ($t = 4.1$, $P < 0.01$) than on either side ($77 \pm 19\%$ in the north; $75 \pm 18\%$ in the south). Lower microzooplankton grazing impact on diatoms in the frontal zone suggests that other diatom loss processes, such as sinking and/or mesozooplankton grazing, were relatively more important there than north or south of the front. Enhanced carbon export in the front zone is implied from the elevated production of heterotrophic bacteria at depths within and below the diatom patch where microbial remineralization of sinking particles takes place (Samo *et al.*, 2012). Vertically integrated standing stocks of mesozooplankton in the upper 100 m were elevated compared with either side of the front (Ohman *et al.*, 2012), also implying their increased role as grazers there.

Biogenic carbon production at the frontal zone

Our model predicts that high carbon biomasses of phytoplankton should be found on the north side of the A-Front, extending from the surface to the bottom of the euphotic zone and penetrating southward and downward across the front along the sloping isopycnals at the frontal zone (Fig. 7). Diatoms contributed a larger fraction (>30%) of phytoplankton carbon biomass north of the front than south, and were particularly prominent in the frontal zone (>50%). The detailed vertical patterns of carbon biomass from our model agree well with the independently derived distributions of beam transmission voltage from CTD profiles (an indicator of particle concentration) and, to some extent, with autotrophic biomass from microscopic observation (Fig. 7). The compromise between model complexity and the accuracy of model predictions is a common challenge faced by ecosystem/biogeochemical modelers during data-model comparisons. Our results here suggest that with appropriate (*a priori*) parameterizations, a simple diagnostic model can accurately reproduce the details of planktonic ecosystem dynamics in the ocean. Application of such models in field studies can substantially improve our understanding of ecosystem patterns

and responses and enhance the utility of the data derived from field observations.

Primary production is the product of the phytoplankton growth rate and carbon biomass. According to the estimates from our model, depth-integrated primary production for the upper 100 m was higher to the north (0.86 ± 0.07 g C m^{-2} day^{-1}) than the south (0.59 ± 0.06 g C m^{-2} day^{-1}) of the front, but highest overall at the frontal interface ($\sim$0.93 g C m^{-2} day^{-1}) (Fig. 6f). These rates are within the range of 0.6–1.1 g C m^{-2} day^{-1} measured in ^{14}C uptake experiments during CalCOFI studies at the same location in the SCCS (near CalCOFI station 87.70; from 2000 to 2006), but do not capture the measured rate disparity in experiments conducted in southern and northern waters (0.35 versus 1.67 g C m^{-2} day^{-1}) adjacent to the front on the present cruise (Landry *et al.*, 2012; Ohman *et al.*, 2012). However, upper 20 m nitrate concentrations during the northern production experiments (1.74 ± 0.43 μM) were substantially higher than those measured on the A-Front transect (0.31 ± 0.13 μM). Modeled *f*-ratios, the ratio of nitrate-based production to total primary production in surface waters were generally higher north of the A-Front ($\sim$0.14) than to the south ($\sim$0.07), which is expected from the lower nutrient fluxes in the south. In the deep chlorophyll maximum south of the front however, predicted *f*-ratios exceeded 0.34, consistent with the observation of high diapycnal nitrate fluxes there.

New production, the portion of primary production fueled by nitrate (plus nitrogen fixation), was estimated to be $\sim$0.15 g C m^{-2} day^{-1} integrated over the euphotic zone at the frontal zone, with an average *f*-ratio of $\sim$0.17. Generally, new production was higher to the north of the front (0.17 ± 0.04 g C m^{-2} day^{-1}) than the south (0.10 ± 0.04 g C m^{-2} day^{-1}). The predicted new production is higher than the value of $\sim$0.05 g C m^{-2} day^{-1} commonly observed in open-ocean ecosystems (Eppley and Peterson, 1979; Lewis *et al.*, 1986) but lower than the new production of $\sim$0.5 g C m^{-2} day^{-1} in coastal waters (e.g. Eppley and Peterson, 1979; Eppley, 1992; Allen *et al.*, 2005). Estimated new production at the frontal zone from our models was about half the estimate of $\sim$0.28 g C m^{-2} day^{-1} that could be supported by the calculated diapycnal nitrate fluxes from below. This result suggests that the diapycnal diffusion of nitrate alone is sufficient to support the amount of new production observed in the frontal zone.

Physical and biological interactions at frontal zones

Subsurface patches of phytoplankton biomass are common features of oceanic fronts. However, hypothesized mechanisms for the formation and maintenance of such patches are diverse and difficult to quantify (e.g. Holligan *et al.*, 1984; Franks, 1992a; Claustre *et al.*, 1994; Levy *et al.*, 2001). Theoretical models indicate that physical processes such as convergence and divergence of cross-frontal flows can concentrate swimming organisms at fronts even without a contribution from growth enhancement (Franks, 1992b). Hood *et al.* (Hood *et al.* 1991) have also suggested that subduction of phytoplankton along isopycnals to deeper nutrient-rich layers along with photoadaptation at lower euphotic zone can lead to diatom aggregations at fronts and filaments in the north California coastal transition zone. Field studies have indicated, however, that high pigment biomass at fronts does not necessarily result from pure physical accumulation but rather from locally enhanced biological production in response to increased diapycnal or isopycnal nutrient fluxes (e.g. Hitchcock *et al.*, 1993; Claustre *et al.*, 1994), possibly combined with reduced grazing pressure (Holligan *et al.*, 1984).

Our analyses of the data collected during the A-Front study, combined with diagnostic model analyses suggest that the elevated phytoplankton biomass in the frontal zone was caused by diapycnal nitrate fluxes that locally enhanced growth and by reduced grazing losses to microzooplankton. These resulted in net positive community production, eventually leading to accumulation of biomass in the frontal zone. The small-scale vertical diffusive flux of nitrate at the front was likely caused by a combination of wind forcing and ageostrophic frontal circulations. The reduced specific grazing mortality rate of phytoplankton in the frontal zone, however, is a result of phytoplankton growth exceeding the grazing capacity. Phytoplankton patches/or blooms at fronts may thus represent areas in which there is a failure of the microzooplankton grazers to contain the higher phytoplankton productivity supported by enhanced nutrient fluxes.

Compared with the small phytoplankton, fast-growing diatoms apparently took advantage of the increased nutrient fluxes to dominate phytoplankton biomass in the frontal zone. Generally, diatoms require nutrient-rich conditions to rise so prominently (e.g. Hutchins and Bruland, 1998; Allen *et al.*, 2005; Kemp *et al.*, 2006). Some large diatoms are also capable of growing in low-light environments, such as the lower euphotic zone, where they are exposed to higher nutrient concentrations (Goldman and McGillicuddy, 2003). In oligotrophic regions, however, diatoms are considered less competitive at low nutrient concentrations than small phytoplankton that have higher surface to volume ratios, and are thus less diffusion limited

(Kiørboe, 1993). It is possible that the biomass of the smaller (non-diatom) phytoplankton was more strongly constrained by their grazers than the larger (diatom) phytoplankton, allowing them to bloom (e.g. Poulin and Franks, 2010). Such dynamics could be revealed through size-resolved estimates of growth and grazing.

Both bottom-up (limiting nutrients) and top-down controls (grazers) play important roles in regulating phytoplankton biomass and community structure (McQueen *et al.*, 1989, Poulin and Franks, 2010). Quantifying the relative importance of these two factors is difficult for dynamic marine ecosystems. The interplay of these two mechanisms in the ocean is spatially and temporally dependent (Hunt and McKinnell, 2006). Our findings suggest that phytoplankton patchiness at frontal zones in the SCCS results from the combined effects of bottom-up and top-down controls on the phytoplankton community. Enhanced diapycnal fluxes of nutrients at the frontal zones increase phytoplankton primary and new production, and this effect, together with reduced microzooplankton grazing (proportional to the phytoplankton community), results in net positive growth and biomass accumulation of large phytoplankton such as diatoms in the frontal zone.

ACKNOWLEDGEMENTS

We thank the CCE-LTER team for their support during the field work. We thank Jennifer MacKinnon for her help on the Thorpe scale analyses.

FUNDING

This work was supported by U. S. National Science Foundation grants OCE 04-17616 and 10-26607 to the CCE Program.

REFERENCES

Allen, J. T., Brown, L., Sanders, R. *et al.* (2005) Diatom carbon export enhanced by silicate upwelling in the northeast Atlantic. *Nature*, **437**, 728–732.

Brink, K. H., Beardsley, R. C., Niiler, P. P. *et al.* (1991) Statistical properties of near-surface flow in the California coastal transition zone. *J. Geophys. Res.*, **96**, 14693–14706.

Claustre, H., Kerherve, P., Marty, J. C. *et al.* (1994) Phytoplankton dynamics associated with a geostrophic front: ecological and biogeochemical implications. *J. Mar. Res.*, **52**, 711–742.

D'Asaro, E., Lee, C., Rainville, L. *et al.* (2011) Enhanced turbulence and energy dissipation at ocean fronts. *Science*, **332**, 318–322.

Davis, R. E., Ohman, M. D., Rudnick, D. L. *et al.* (2008) Glider surveillance of physics and biology in the southern California Current System. *Limnol. Oceanogr.*, **53**, 2151–2168.

Eppley, R. W. (1992) Chlorophyll, photosynthesis and new production in the Southern California Bight. *Prog. Oceanogr.*, **30**, 117–150.

Eppley, R. W. and Peterson, B. J. (1979) Particulate organic matter flux and planktonic new production in the deep ocean. *Nature*, **282**, 677–680.

Franks, P. J. S. (1992a) Phytoplankton blooms at fronts: patterns, scales and physical forcing mechanisms. *Rev. Aqua. Sci.*, **6**, 121–137.

Franks, P. J. S. (1992b) Sinking and swim: accumulation of biomass at fronts. *Mar. Ecol. Prog. Ser.*, **82**, 1–12.

Franks, P. J. S. and Walstad, L. J. (1997) Phytoplankton patches at fronts: a model of formation and response to wind events. *J. Mar. Res.*, **55**, 1–29.

Galbraith, P. S. and Kelley, D. E. (1996) Identifying Overturns in CTD Profiles. *J. Atmos. Ocean. Tech.*, **13**, 688–702.

Gargett, A. E. and Garner, T. (2008) Determining Thorpe scales from ship-lowered CTD density profiles. *J. Atmos. Ocean. Tech.*, **25**, 1657–1670.

Gasol, J. M., del Giorgio, P. A. and Duarte, C. M. (1997) Biomass distribution in marine planktonic communities. *Limnol. Oceanogr.*, **42**, 1353–1363.

Goldman, J. C. and McGillicuddy, D. J. (2003) Effect of large marine diatoms growing at low light on episodic new production. *Limnol. Oceanogr.*, **48**, 1176–1182.

Gregg, M. C. (1989) Scaling turbulent dissipation in the thermocline. *J. Geophys. Res.*, **94**, 9686–9698.

Hales, B., Moum, J. N., Covert, P. *et al.* (2005) Irreversible nitrate fluxes due to turbulent mixing in a coastal upwelling system. *J. Geophy. Res.*, **110**, C10S11, doi:10.1029/2004JC002685.

Hitchcock, G. L., Mariano, A. J. and Rossby, T. (1993) Mesoscale pigment fields in the Gulf Stream: observations in a meander crest and trough. *J. Geophys. Res.*, **948**, 8425–8445.

Holligan, P. M., Williams, P. J., Purdie, D. *et al.* (1984) Photosynthesis, respiration and nitrogen supply of plankton populations in stratified, frontal and tidally mixed shelf waters. *Mar. Ecol. Prog. Ser.*, **17**, 201–213.

Hood, R. R., Abbott, M. R. and Huyer, A. (1991) Phytoplankton and photosynthetic light response in the coastal transition zone off northern California in June 1987. *J. Geophys. Res.*, **96**, 14769–14780.

Hoskins, B. J. (1974) The role of potential vorticity in symmetric stability and instability. *Quart. J. Roy. Meteor. Soc*, **100**, 480–482.

Hunt, G. L. and McKinnell, S. (2006) Interplay between top-down, bottom-up, and wasp-waist control in marine ecosystems. *Prog Oceanogr.*, **68**, 115–124.

Hutchins, D. A. and Bruland, W. W. (1998) Iron-limited diatom growth and Si:N uptake ratios in a coastal upwelling regime. *Nature*, **393**, 561–564.

Kahru, M., DiLorenzo, E. and Manzano-Sarabia, M. (2012) Spatial and temporal statistics of sea surface temperature and chlorophyll fronts in the California current. *J. Plank. Res.*, **34**, 749–760.

Kemp, A. E. S., Pearce, R. B., Grigorov, I. *et al.* (2006) Production of giant marine diatoms and their export at oceanic frontal zones: Implication for Si and C flux from stratified oceans. *Glob. Biogeochem. Cyc.*, **20**, GB4S04. , doi:10.1029/2006GB002698.

Kiørboe, T. (1993) Turbulence, phytoplankton cell size, and the structure of plelagic food webs. *Adv. Mar. Biol.*, **29**, 1–72.

Landry, M. R., Ohman, M. D. and Goericke, R. (2009) Lagrangian studies of phytoplankton growth and grazing relationships in a coastal upwelling ecosystem off Southern California. *Prog. Oceanogr.*, **83**, 208–216.

Landry, M. R., Ohman, M. D., Goericke, R. *et al.* (2012) Pelagic community responses to a deep-water frontal system in the California Current Ecosystem: overview of the A-Front study. *J. Plank. Res.*, **34**, 739–748.

Law, C. S., Abraham, E. R., Watson, A. J. *et al.* (2003) Vertical eddy diffusion and nutrient supply to the surface mixed layer. *J. Geophys. Res.*, **108**, C001604, doi:10.1029/2002JC001604.

Ledwell, J. R., McGillicuddy, D. J. and Anderson, L. A. (2008) Nutrient flux into an intense deep chlorophyll layer in a mode-water eddy. *Deep Sea Res., Part II*, **55**, 1139–1160.

Levy, M., Klein, P. and Treguier, A. (2001) Impact of sub-mesoscale physics on production and subduction of phytoplankton in an oligotrophic regime. *J. Mar. Res.*, **59**, 535–565.

Lewis, M. R., Harrison, W. G., Oakey, N. S. *et al.* (1986) Vertical nitrate fluxes in the oligotrophic ocean. *Science*, **234**, 870–873.

Li, Q. P., Franks, P. J. S., Landry, M. R. *et al.* (2010) Modeling phytoplankton growth rates and Chlorophyll to Carbon ratios in California coastal and pelagic ecosystems. *J. Geophys. Res.*, **115**, G04003, doi:10.1029/2009jg001111.

Li, Q. P., Franks, P. J. S. and Landry, M. R. (2011) Microzooplankton grazing dynamics: parameterizing grazing models with dilution experiment data in the California Current Ecosystem. *Mar. Ecol. Prog. Ser.*, **438**, 59–69.

Li, Q. P., Hansell, D. A., McGillicuddy, D. J. *et al.* (2008) Tracer based assessment of the origin and biogeochemical transformation of a cyclonic eddy in the Sargasso Sea. *J. Geophys. Res.*, **113**, C10006, doi:10.1029/2008jc004840.

Mahadevan, A. and Tandon, A. (2006) An analysis of mechanisms for submesoscale vertical motion at ocean fronts. *Ocean Modeling*, **14**, 241–256.

McGillicuddy, D. J., Anderson, L., Bates, N. *et al.* (2007) Eddy-wind interactions stimulate extraordinary mid-ocean plankton blooms. *Science*, **316**, 1021–1026.

McQueen, D. J., Johannes, M. R. S., Post, J. R. *et al.* (1989) Bottom-up and top-down impacts on freshwater pelagic community structure. *Ecological Monographs*, **59**, 289–309.

Mooers, C. N. K. and Robinson, A. R. (1984) Turbulent jets and eddies in the California Current and inferred cross-shore transports. *Science*, **223**, 51–53.

Munk, W. and Wunsch, C. (1998) Abyssal Recipes II: energetics of tidal and wind mixing. *Deep Sea Res.*, **45**, 1977–2010.

Ohman, M. D., Powell, J., Picheral, M. *et al.* (2012) Mesozooplankotn and particulate matter response to a deep-water frontal system in the southern California Current System. *J. Plank. Res.*, **34**, 815–827.

Osborn, T. R. (1980) Estimation of the local rate of vertical diffusion from dissipation measurements. *J. Phys. Oceanogr.*, **10**, 83–89.

Partensky, F., Hess, W. R. and Vaulot, D. (1999) *Prochlorococcus*, a marine photosynthetic prokaryote of global significance. *Microbiol. Mol. Biol. Rev.*, **63**, 106–127.

Poulin, F. J. and Franks, P. J. S. (2010) Size-structured planktonic ecosystem dynamics: constraints, controls and assembly instructions. *J. Plankton Res.*, **32**, 1121–1130.

Samo, T., Pedler, B., Ball, I. *et al.* (2012) Microbial distribution and activity across a water mass frontal zone in the California Current Ecosystem. *J. Plank. Res.*, **34**, 802–814.

Taylor, A. G., Goericke, R., Landry, M. R. *et al.* (2012) Sharp gradients in phytoplankton community structure across a frontal zone in the California current system. *J. Plank. Res.*, **34**, 778–789.

Thingstad, T. F., Krom, M. D., Mantoura, R. F. C. *et al.* (2005) Nature of phosphorus limitation in the ultraoligotrophic eastern Mediterranean. *Science*, **309**, 1068–1071.

Thomas, L. N. and Taylor, J. R. (2010) Reduction of the usable wind-work on the general circulation by forced symmetric instability. *Geophys. Res. Lett.*, **37**, L18606, doi:10.1029/2010GL044680.

Thompson, A. F., Gille, S. T., Mackinnon, J. A. *et al.* (2007) Spatial and temporal patterns of small-scale mixing in Drake Passage. *J. Phys. Oceanogr.*, **37**, 572–592.

Thorpe, S. A. (1977) Turbulence and mixing in a Scottish loch. *Phil. Trans. Royal Soc., London A*, **286**, 125–181.

Yoder, J. A., Ackleson, S. G., Barber, R. T. *et al.* (1994) A line in the sea. *Nature*, **371**, 689–692.